SUPPLEMENT: Measuring Decadal Vertical Land-level Changes from SRTM-C (2000) and TanDEM-X (~2015) in the South-Central Andes

Benjamin Purinton[1] and Bodo Bookhagen[1]

[1]Institute of Earth and Environmental Science, Universität Potsdam, Potsdam, Germany

Correspondence: Ben Purinton (purinton@uni-potsdam.de)

S1 TanDEM-X and SRTM-C Internal Error Exploration

TanDEM-X tiles are delivered with a number of auxiliary layers allowing deeper exploration of errors. The detailed description of each layer can be found in the product technical document (Wessel, 2016). In general we expect the TanDEM-X to have superior accuracy to previous datasets given the fine raw radiometric resolution (~3.3 m) combined with the high number of contributing scenes per pixel (Fig. S1). Vertical uncertainties from our extensive differential GPS (dGPS) control dataset (Purinton and Bookhagen, 2017) revealed the dependence of vertical uncertainty on both consistency of the input scenes (COM) and the height error map (HEM). The HEM contains expected random error (in meters) for each pixel and is typically larger over less coherent areas like vegetation or water (Wessel et al., 2018). The COM demonstrates the agreement between individual scenes, providing information about pixels which had potential contribution from poor performance TerraSAR-X / TanDEM-X looks. Figures S2–S3 demonstrate these errors compared with sub-20 cm vertical accuracy dGPS points.

The dependence of TanDEM-X error on terrain slope is demonstrated in Figure S4, where we note worsening vertical error with increasing slope and apparent over-prediction of TanDEM-X heights. We see this same trend in the SRTM-C data compared with dGPS (Fig. S5). Since both DEMs are over-predicting heights on steeper slopes in the same way, we expect the relative difference between each to remain the same for the mapping of vertical land-level changes. We note the dearth of height measurements on higher slopes, however, this positive relationship for TanDEM-X is also found by Wessel et al. (2018).

In Figure S6 we explore the relation between HEM and slope including information from the water indication mask (WAM) from TanDEM-X. The WAM is based on amplitude and coherence thresholds (Wendleder et al., 2013) and may therefore contain additional information besides water pixels, such as areas that lost coherence in deserts or very steep and vegetated slopes (Fig. 1C, main text). From Figure S6, we note that the very high HEM values at low slopes are reduced when removing pixels identified as having low amplitude or coherence. While these are largely water bodies in TanDEM-X, they also correspond to DEM artifacts on hillslopes and in salt flats. We can observe a non-linear trend with increasing slope and vertical uncertainty, which we also see in the boxplots of Figures S4–S5.

S2 TanDEM-X and SRTM-C Differencing Errors

In addition to comparison with dGPS and TanDEM-X auxiliary layers, we also examine the dependence on TanDEM-X−SRTM-C dh on a number of terrain characteristics. These biases could affect dh change mapping and measurement and therefore warrant special attention. Figure S7A demonstrates the expected increase in uncertainty with slope, however, since both the DEMs over-predict heights at higher slopes in the same manner, we do not observe any linear trends in differencing these datasets at higher slopes. Figure S7B shows that this increase in uncertainty is also related to relief (which increases with higher slopes as well), though local relief has a smaller effect on uncertainty.

Since slope and relief may overprint other biases, we also test the dependence of dh on elevation (Fig. S8) and vegetation (Fig. S9) on only low slope and low relief terrain using cutoffs of 5° and 100 m, respectively. Since most high slope and high relief terrain is found in the steep topographic transition zone at the mountain front (Fig. 1, main text), this threshold removes all elevations in this band (~1800–2500 m). This orographic mount-front band also corresponds to moderate vegetation, thus only the very low (Altiplano-Puna Plateau) and very high (wet foreland) vegetation values are shown. We note no trends in either vegetation or elevation. Although we would expect vegetation differences between X-band and C-band, it may be the case that sub-tropical forests in the region are not dense enough to fully block radar penetration over a significant number of pixels.

Despite having the same nominal resolution of 1 arcsec, the SRTM-C and TanDEM-X demonstrate clear differences in raw radiometric resolution (~30 m versus ~3.3 m) when comparing plots of terrain curvature versus dh (Fig. S10). Many studies of glacier height change apply a polynomial correction to height values based on this relationship (e.g., Gardelle et al., 2012; Ruiz et al., 2017), however, this introduces artificial elevations, whereas we are interested in the raw data. Furthermore, this curvature bias only affects the most peaked and narrowest parts of the landscape, whereas the more planar regions (e.g., gravel-bed channels, landslide lobes) show less error dependence on curvature.

S3 Relation of Destriped Block Median dh to Elevation

Following our non-aggressive (97.5^{th} percentile cutoff and 5% RMSE convergence) FFT destriping, a number of patches of positive and negative dh remain. Though these patches were removed in a more aggressive approach (95^{th} percentile cutoff and 2% RMSE convergence), this method also filtered true topography (Fig. S11). We instead rectified these patches using the blocked shifting scheme discussed in the main text Section 4.1.3. We did not find any clear relation between the medians in each block or elevation for any of the block sizes tested (Fig. S12). Rather the remaining error patterns were likely caused by a complex combination of remaining SRTM-C orbital biases, atmospheric conditions at the time of SRTM-C capture, local adjustment of both datasets to ICESat measurements, and possibly the over-prediction of elevation in both datasets on steep topography (Fig. S4–S5).

S4 Increase in dh Measurements Downstream of Knickpoints

As mentioned in the main text, there is a clear increase in number of measurements downstream of the knickpoint for the Río Grande and Río Toro. The 2D KDE shown in main text Figure 7 does not provide the downstream number of measurements, but is rather a demonstration of relative point density. In Figure S13, we demonstrate the 1 km binned measurements downstream using a simple histogram plot. Here we see the increase in number of measurements in the wider, downstream channel reaches.

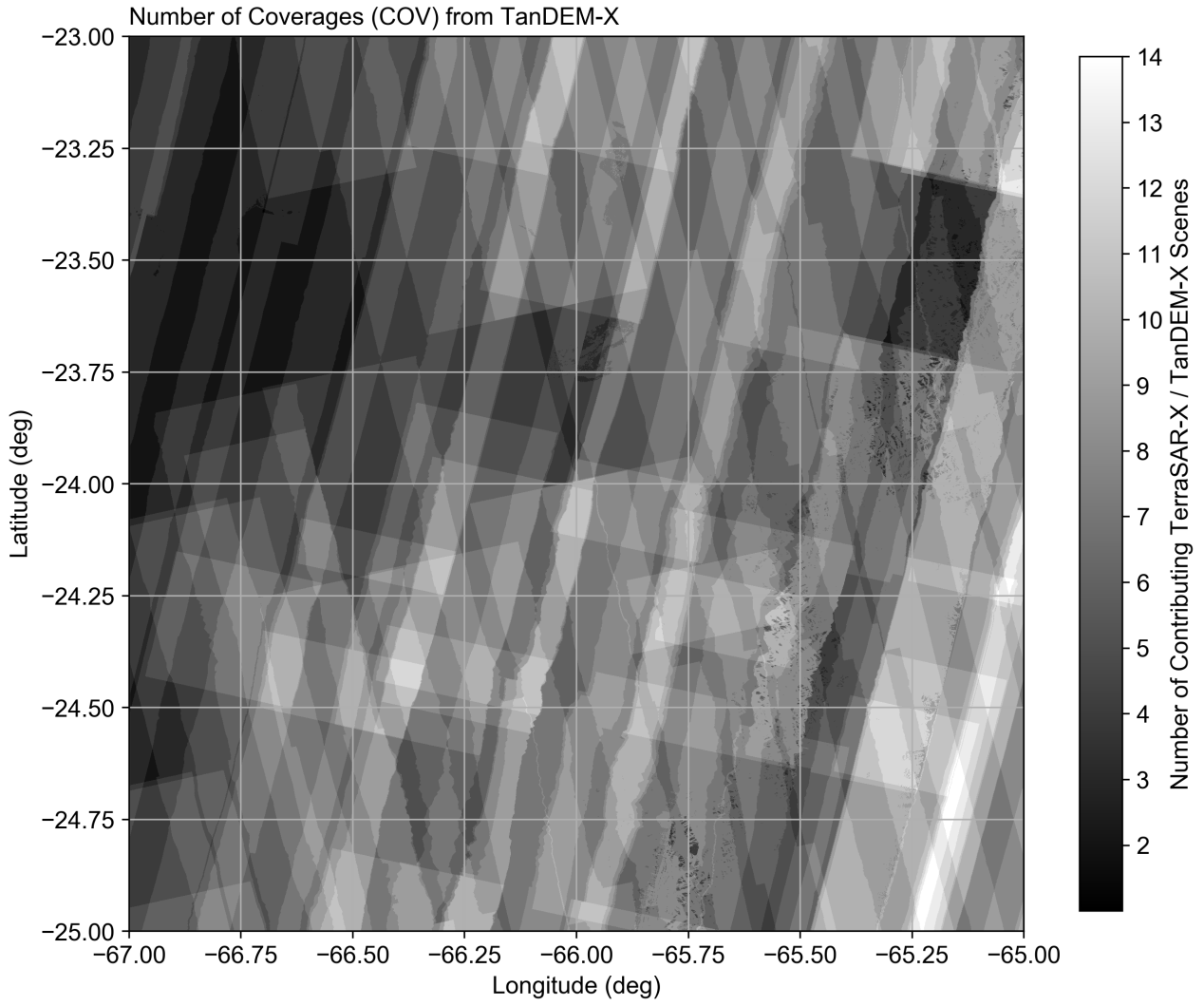

Figure S1. Coverage map (COV) for four tiles of TanDEM-X (S 24–25°, W 66–67°). Note high number of coverages up to 14 on eastern side where topography is steeper, versus less coverage to west on Altiplano-Puna low-relief plateau.

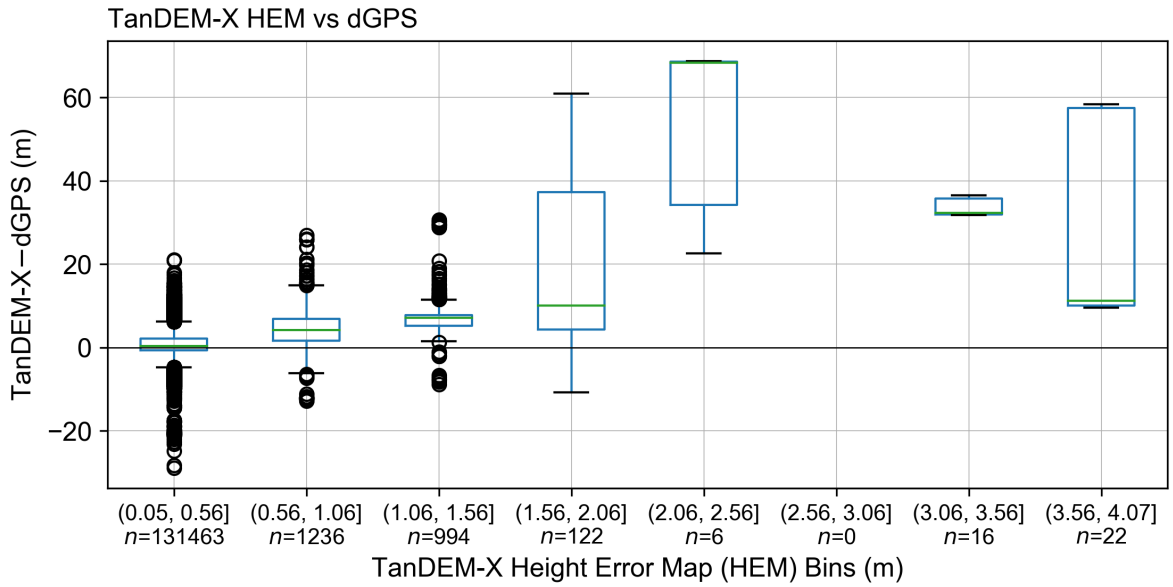

Figure S2. Height error map (HEM) values binned in 0.5 m intervals with boxplots showing TanDEM-X elevation compared with dGPS measurements. Note number of measurements (n) at higher HEM values drops significantly. Similar to Wessel et al. (2018) we observe a positive trend in vertical uncertainty with HEM and much worse accuracy at HEM values > 0.5 m. These higher HEM values also correspond to higher slopes, indicating the over-prediction of TanDEM-X at extreme slopes (cf. Fig. S4).

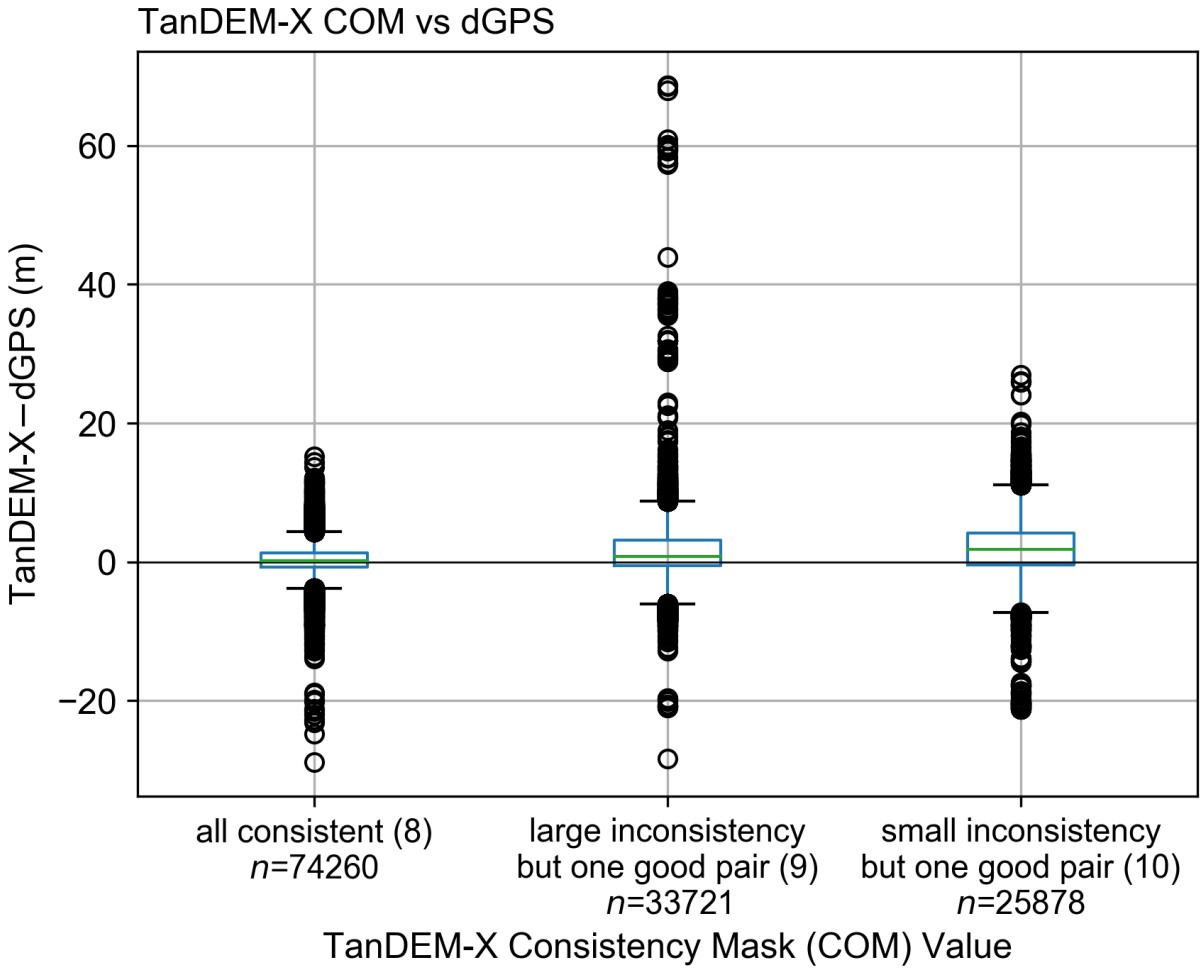

Figure S3. Consistency map (COM) boxplots of TanDEM-X vertical uncertainty versus dGPS for all COM values covered, and the meaning of each COM value. See Wessel (2016) for detailed description of each COM value. We note a greater vertical uncertainty with more inconsistent COM values, whereas for COM value 8 (all input heights consistent), the vertical uncertainty boxplot is narrow and centered on zero median.

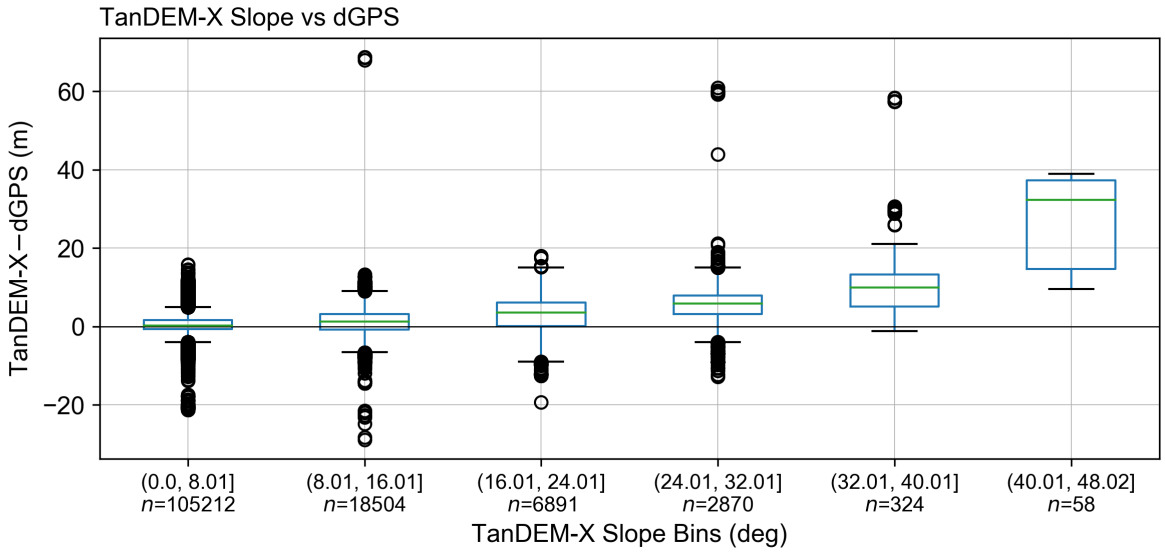

Figure S4. Terrain slope binned in 8° intervals versus boxplots of dGPS vertical uncertainty for TanDEM-X. We note worsening vertical uncertainty at higher slopes and an apparent over-prediction of heights by TanDEM-X. Note the drop in number of measurements (n) at higher slopes.

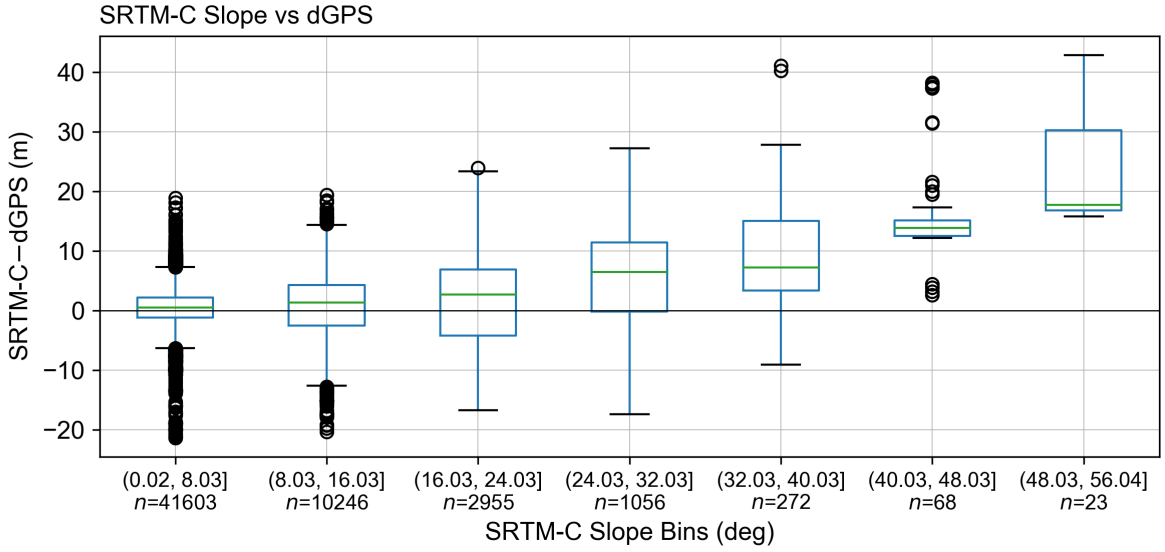

Figure S5. Terrain slope binned in 8° intervals versus boxplots of dGPS vertical uncertainty for SRTM-C. We note worsening vertical uncertainty at higher slopes and an apparent over-prediction of heights by SRTM-C. Note the drop in number of measurements (n) at higher slopes.

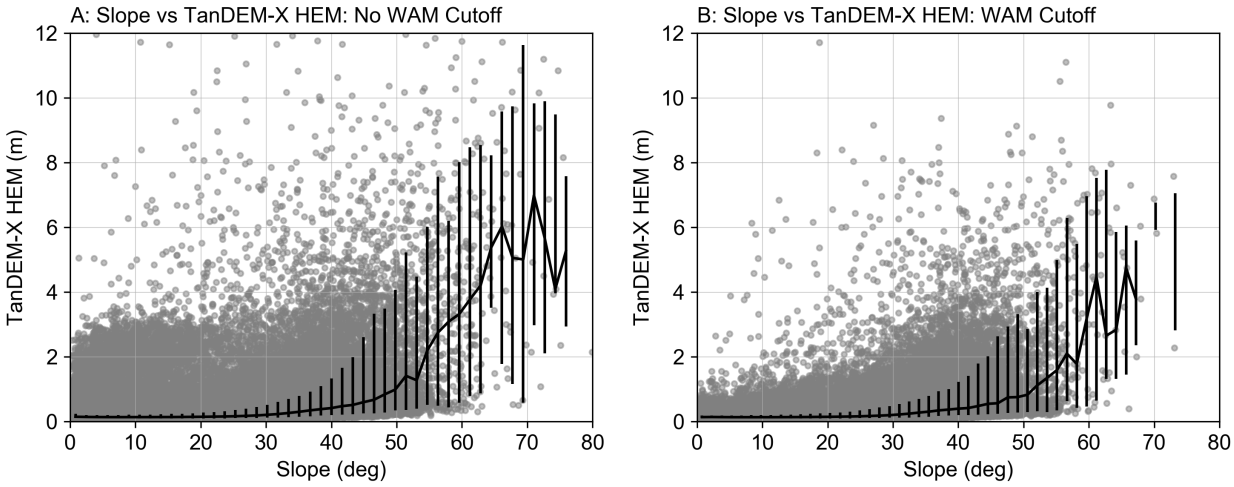

Figure S6. Terrain slope versus HEM for TanDEM-X. Gray points are raw data and black line is median values with 10^{th} and 90^{th} percentile error bars. (A) is all pixels including those with low amplitude and coherence, whereas in (B) the WAM cutoff is applied to remove these pixels. Note the reduction of high HEM outliers at primarily lower slopes (water bodies) with WAM cutoff.

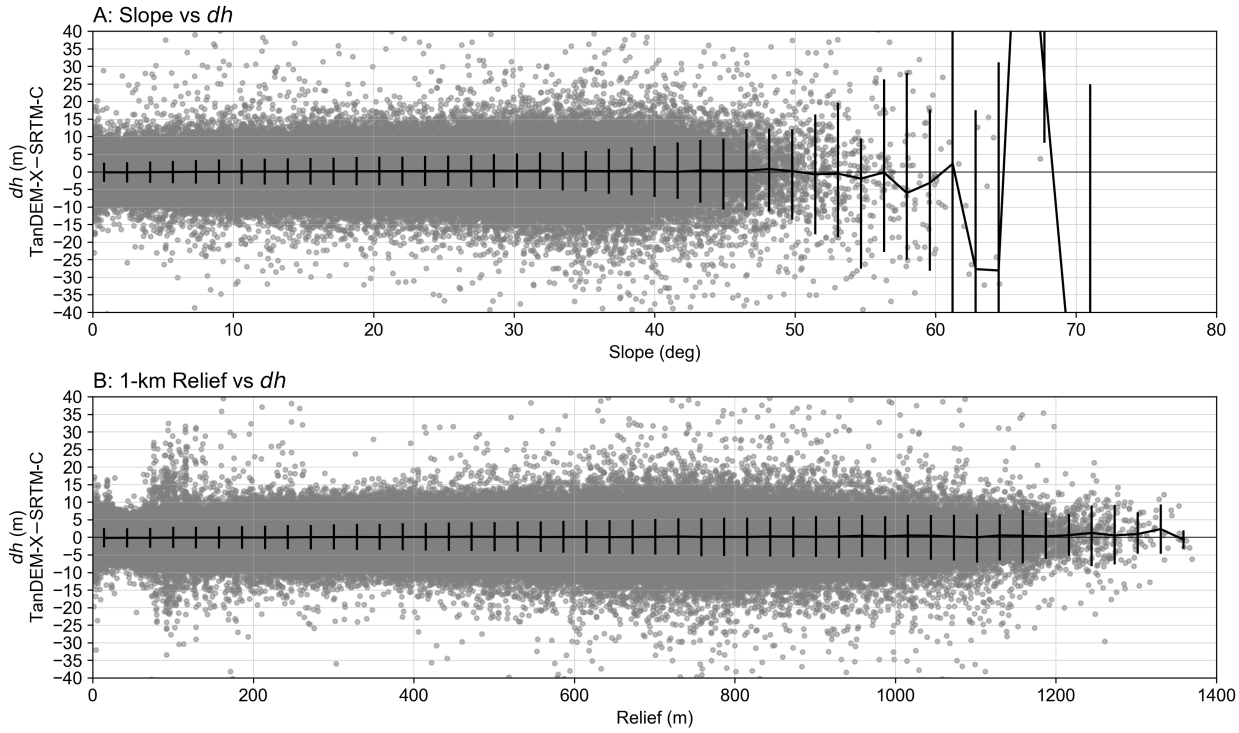

Figure S7. (A) Terrain slope versus dh and (B) 1-km relief versus dh. Gray points are raw data and black line is median values with 10^{th} and 90^{th} percentile error bars. Aside from greater uncertainties at higher slopes, we note no linear trend with either parameter that may affect dh identification.

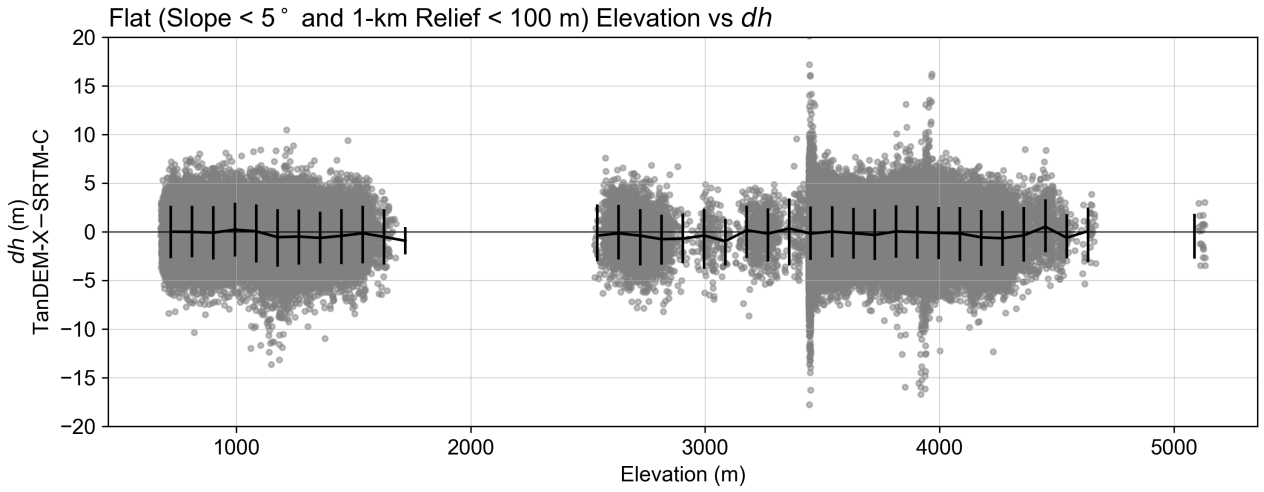

Figure S8. Terrain elevation versus dh. Gray points are raw data and black line is median values with 10^{th} and 90^{th} percentile error bars. All elevations in the high slope and high relief topographic transition zone (~1800–2500) have been filtered out.

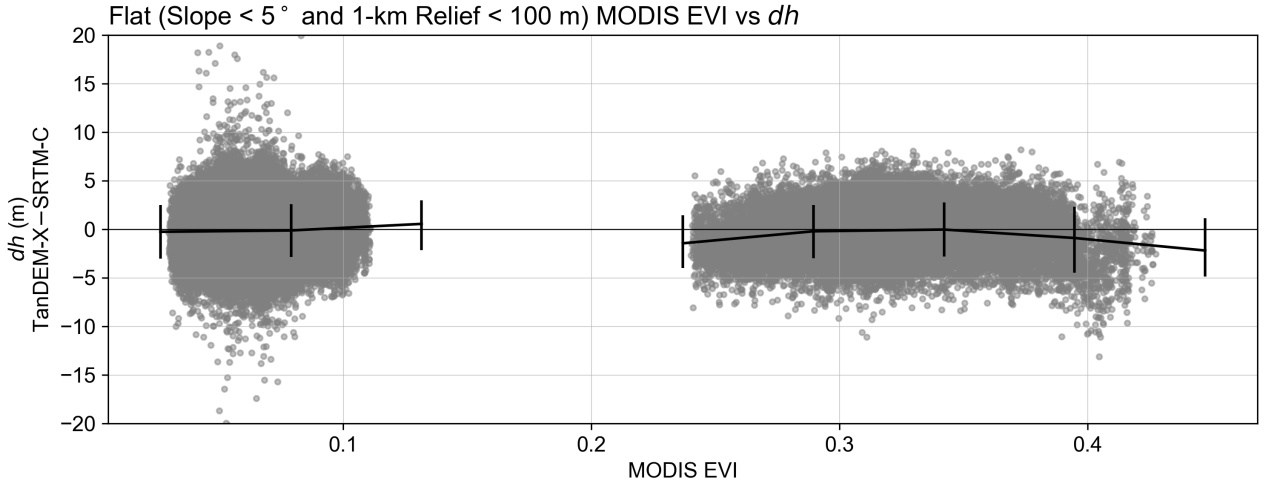

Figure S9. Vegetation versus dh. We use enhanced vegetation index (EVI) from MODIS product MOD13C1 (Huete et al., 1994) averaged over 14 years to track vegetation (Fig. 1C, main text). Gray points are raw data and black line is median values with 10^{th} and 90^{th} percentile error bars. All elevations in the high slope and high relief topographic transition zone (~1800–2500) have been filtered out.

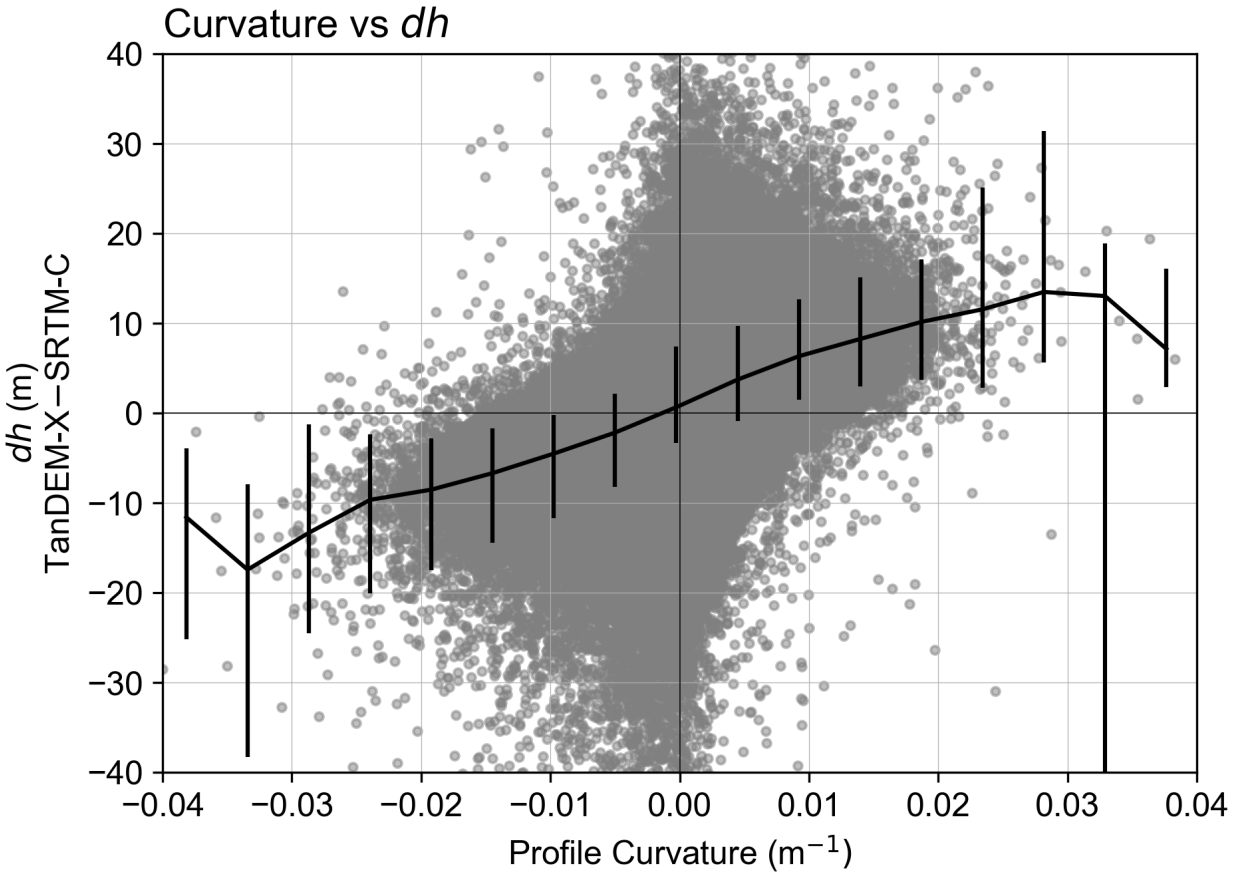

Figure S10. Terrain curvature versus dh. Gray points are raw data and black line is median values with 10^{th} and 90^{th} percentile error bars. Negative (positive) curvature values are valleys (ridges) corresponding to negative (positive) dh values where the SRTM-C is over- (under-) predicting heights.

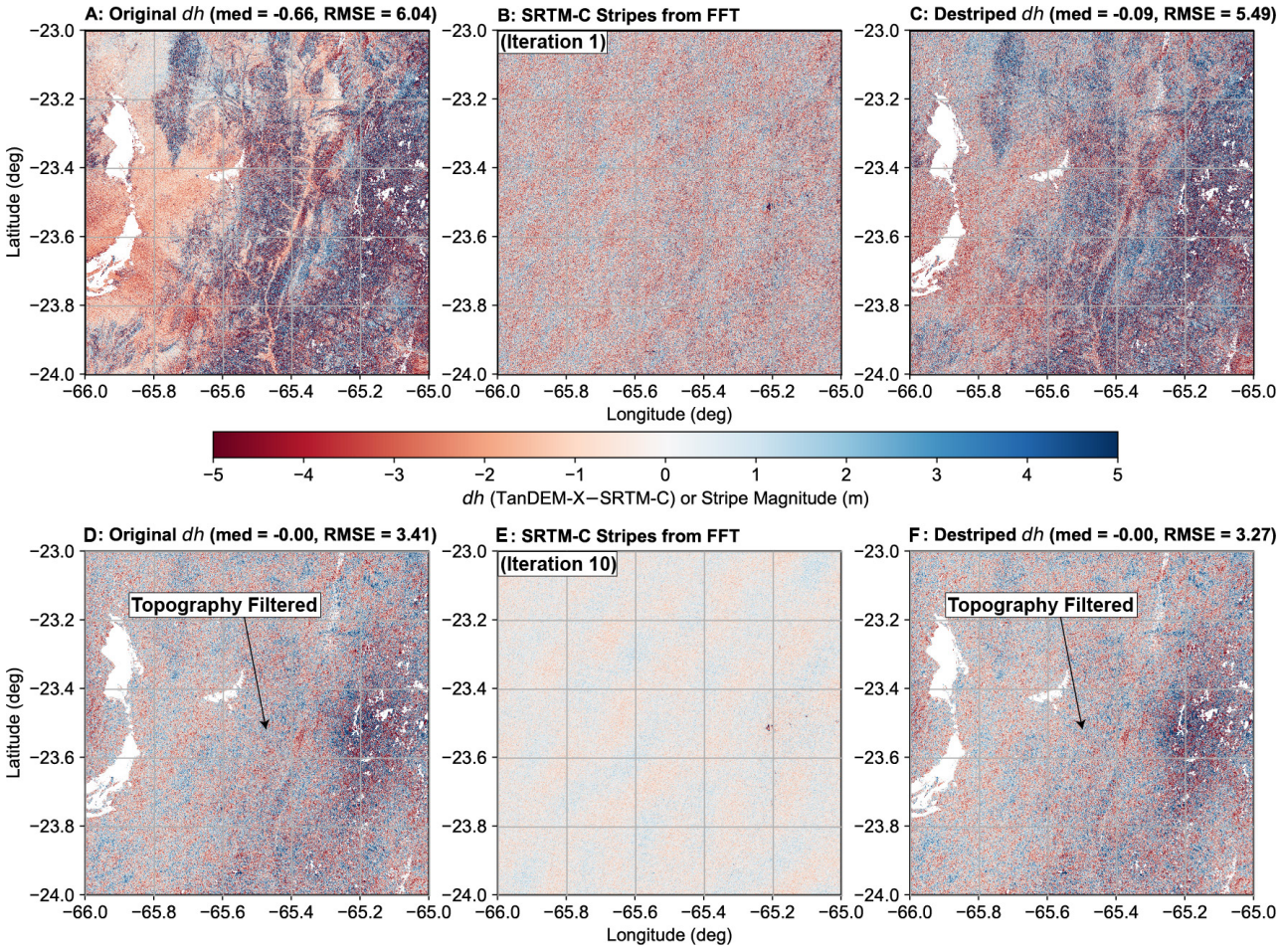

Figure S11. Two iterations of more aggressive FFT destriping from one tile (S 24°, W 66°), same as in main text Figure 3. Top panel (A–C) show first iteration and bottom panel (D–F) show tenth iteration. We note that while the striping and remaining patches caused by SRTM-C collection biases are removed using the more aggressive approach, the true topographic noise is also filtered, which is not the aim of our correction steps.

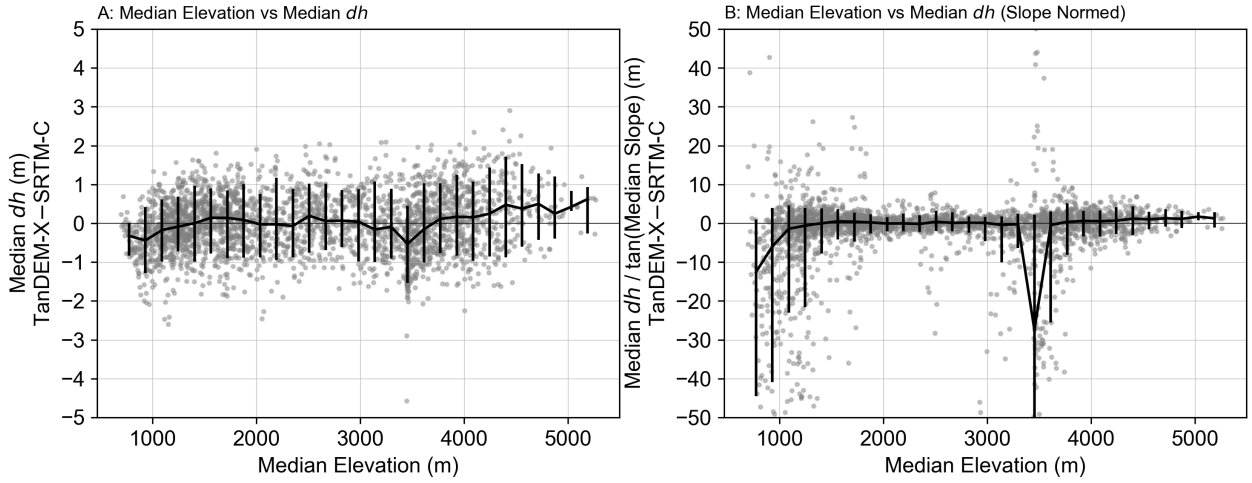

Figure S12. (A) Blocked median elevation versus median dh, and (B) same plot normalized by median slope in each block. Gray points are raw data and black line is median values with 10^{th} and 90^{th} percentile error bars. This is 2700 blocks of size 3.6×3.6 km over three tiles shown in main text Figure 4 (S 24–26°, W 66°). We do not note any distinct trends among the scatter.

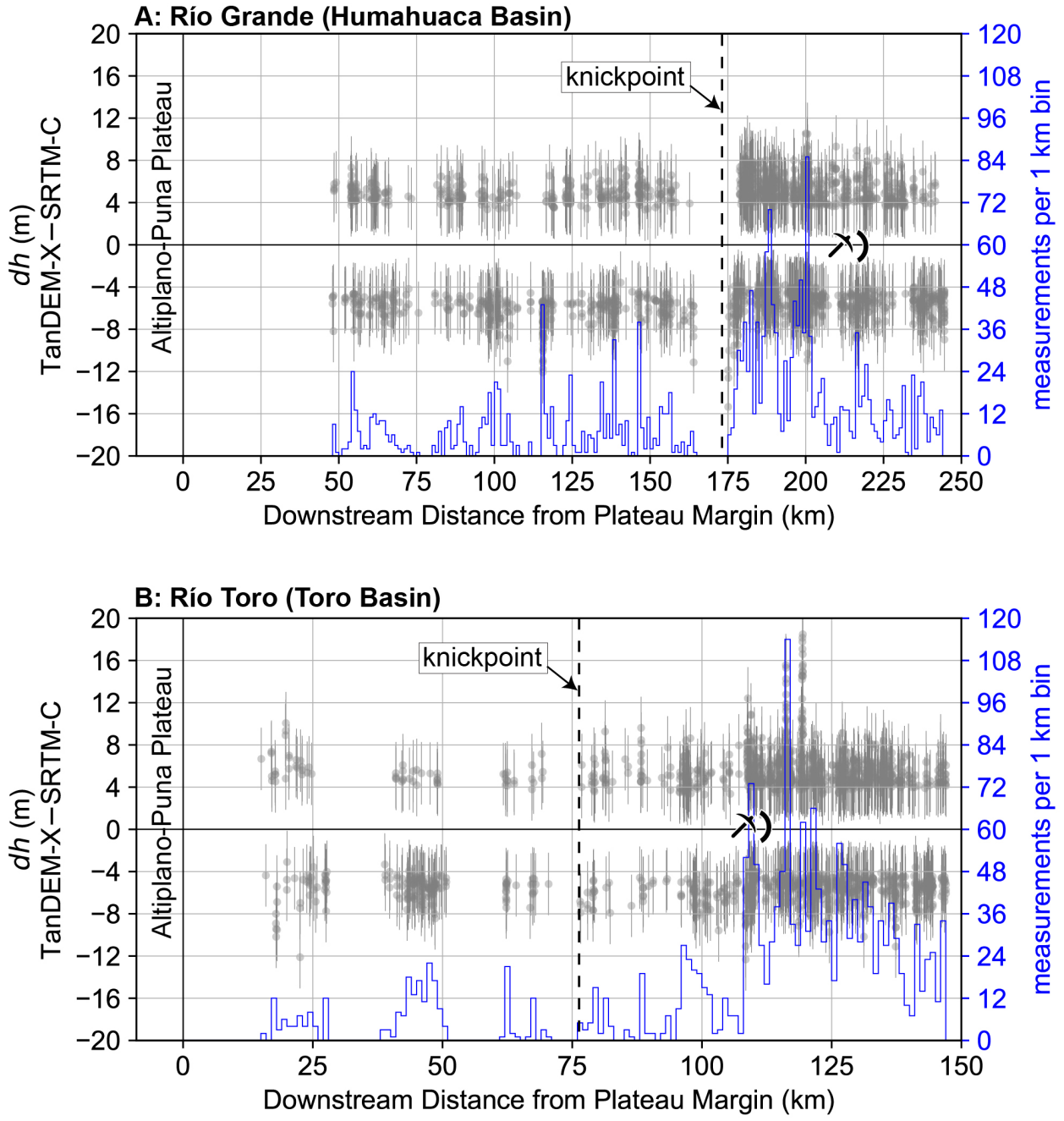

Figure S13. Point clouds (gray points) of potential dh signal (pixels outside of the range of expected noise) plotted with downstream distance for (A) Río Grande and (B) Río Toro. The left axis and points is identical to main text Figure 7. Error bars are RMSE from low slope ($< 5^{\circ}$) terrain outside of the channel area. Rather than coloring each dh point cloud by relative density as in main text Figure 7, here we bin the measurements by 1-km reaches downstream and demonstrate the number of pixels on the right (blue) axis as a histogram. The location of the knickpoint is again indicated, demonstrating the approximately five to ten fold increase in measurements in the downstream reaches of both channels.

References

Gardelle, J., Berthier, E., and Arnaud, Y.: Impact of resolution and radar penetration on glacier elevation changes computed from DEM differencing, Journal of Glaciology, 58, 419–422, https://doi.org/10.3189/2012JoG11J175, 2012.

Huete, A., Justice, C., and Liu, H.: Development of vegetation and soil indices for MODIS-EOS, Remote Sensing of Environment, 49, 224–234, 1994.

Purinton, B. and Bookhagen, B.: Validation of digital elevation models (DEMs) and comparison of geomorphic metrics on the southern Central Andean Plateau, Earth Surface Dynamics, 5, 211, https://doi.org/10.5194/esurf-5-211-2017, 2017.

Ruiz, L., Berthier, E., Viale, M., Pitte, P., and Masiokas, M. H.: Recent geodetic mass balance of Monte Tronador glaciers, northern Patagonian Andes, The Cryosphere, 11, 619, 2017.

Wendleder, A., Wessel, B., Roth, A., Breunig, M., Martin, K., and Wagenbrenner, S.: TanDEM-X water indication mask: Generation and first evaluation results, IEEE Journal of Selected Topics in Applied Earth Observations and Remote Sensing, 6, 171–179, 2013.

Wessel, B.: TanDEM-X Ground Segment–DEM Products Specification Document, Technical Note 3.1, German Aerospace Center (DLR) (Aug.)., 2016.

Wessel, B., Huber, M., Wohlfart, C., Marschalk, U., Kosmann, D., and Roth, A.: Accuracy Assessment of the Global TanDEM-X Digital Elevation Model with GPS Data, ISPRS Journal of Photogrammetry and Remote Sensing, pp. 1–12, 2018.